AIAA Guidance, Navigation, and Control Conference and Exhibit
16 - 19 August 2004, Providence, Rhode Island

AIAA 2004-5024

Effects of Navigation Filter Properties on Formation Flying Control

Megan Mitchell*, Louis Breger*, and Jonathan P. How†
MIT Department of Aeronautics and Astronautics

Kyle T. Alfriend‡
Department of Aeronautics, Texas A&M University

This paper extends previous analysis on the impact of sensing noise for the navigation and control aspects of formation flying spacecraft. We analyze the use of Carrier-phase Differential GPS (CDGPS) in relative navigation filters, with a particular focus on the filter correlation coefficient. This work was motivated by previous publications which suggested that a "good" navigation filter would have a strong correlation (i.e., coefficient near -1) to reduce the semimajor axis error, and therefore, the overall fuel use. However, practical experience with CDGPS-based filters has shown this strong correlation seldom occurs (typical correlations ≈ -0.1), even when the estimation accuracies are very good. We derive an analytic estimate of the filter correlation coefficient and demonstrate that, for the process and sensor noises levels expected with CDGPS, the expected value should be very small. This observation is verified with several linear and nonlinear simulations. Further examples are presented to show that the extended Kalman filter can be forced to create solutions with stronger correlations, but these always result in larger semimajor axis errors. The combination of these simulations and analysis provide new insights on the crucial role of the process noise in determining the semimajor axis knowledge.

I. Introduction

FORMATION flying for spacecraft is an attractive technology for several forthcoming missions.[1,2] This approach has significant advantages over a single spacecraft, such as greater science return due to longer observation baselines, and increased flexibility. The problem of controlling spacecraft in formation is extremely challenging, requiring precise control without excessive fuel use. Recent studies[5,6] have shown that sensing uncertainty is a significant driver of control design. This paper contributes to the field through an investigation of the use of GPS to sense relative orbit states, with particular attention to the differential energy between two orbiting spacecraft, which determines the stability of their formation.

Ref. 4 develops several expressions for analyzing the error in the semimajor axis estimate. This analysis shows that if the relative radial position and in-track velocity estimation errors are highly correlated and appear in the proper ratio, then these errors cancel and the resulting error in the semimajor axis estimate approaches zero. However, experience has shown that when Kalman filters are used with Carrier Phase Differential GPS (CDGPS) measurements, they do not produce highly correlated estimates of the position and velocity states.[10] Ref. 4 thus concluded that GPS-based optimal estimators are typically not "good" navigation filters. We present several simulation results that investigate this point further, and the results show that producing the best estimate of relative semimajor axis using a Kalman filter does not necessarily correspond to producing state estimates with low correlation coefficients (*i.e.,* -1).

This investigation also examines a linear model of GPS sensing that excludes errors introduced by absolute state error, ionosphere, clocks, and carrier phase bias. The linear model is used to gain insights into the

*Research Assistant, MIT Department of Aeronautics and Astronautics
†Associate Professor, MIT Department of Aeronautics and Astronautics, Senior Member AIAA.
‡Professor, Department of Aeronautics, Texas A&M University

fundamental behavior of the filter before adding other real-world effects. This approach is applied to demonstrate that navigation accuracy degrades when the problem statement is changed to force a high correlation between the position and velocity estimates. This provides a counterexample to a previous conjecture that suggests semimajor axis error can effectively be canceled when there is high correlation between position and velocity error.[4] The example is further used to explore how the filter design parameters affect the navigation accuracy. Finally, the mapping between the linear simulations and the full CDGPS-driven simulations is shown to validate conclusions drawn from the linear analysis.

II. Relating Navigational Errors to Semimajor Axis Error

In formation flying missions, accurate knowledge of the difference in semimajor axes, or equivalently, the difference in orbital energy, between the vehicles in the formation is important.[4,5,6] A difference in semimajor axes means that the two vehicles have different orbital periods and thus they will drift out of formation unless considerable control effort is applied.[3] The output of the CDGPS Kalman filter includes the relative formation state in a Local Vertical Local Horizontal (LVLH) reference frame. Understanding the relationship between position and velocity accuracies and semimajor axis accuracy is key to evaluating the output of this type of filter. While Ref. 4 develops the navigation error analysis from absolute state relations, the results can be reformulated for the relative case. The relative navigation error equations, shown below, relate semimajor axis error to position and velocity errors. Note that this discussion is limited to circular reference orbits. The semimajor axis, a, of vehicle i is

$$\frac{1}{\mathrm{a_i}} = \frac{2}{\mathrm{r_i}} - \frac{\mathrm{v_i^2}}{\mu} \tag{1}$$

where r and v are the position and velocity magnitudes in the Earth Centered Inertial (ECI) reference frame, and μ is the gravitational constant of the Earth. Eq. 1 is used to find the difference in semimajor axes of vehicles i and j,

$$\Delta a_{ij} \approx 2(r_j - r_i) + \frac{2}{n}(v_j - v_i) \tag{2}$$

where the vehicles are assumed to be in circular orbits and close to each other. The change in the semi-major axis is caused by a difference in the two radii and the two velocity magnitudes. To first order, the difference in the magnitude of two close vectors is caused by the difference in length along the vector, differences perpendicular to the vector do not change the magnitude of the vector. Consequently, for the radius vector, this is the difference in radial position, and for the velocity, the difference in along track velocity. The radial, in-track, and cross-track directions define the x, y and z axes of the LVLH reference frame. The relative dynamics in this LVLH reference frame are described by Hill's equations,[7]

$$\begin{aligned} \ddot{x} - 2n\dot{y} - 3n^2 x &= f_x \\ \ddot{y} + 2n\dot{x} &= f_y \\ \ddot{z} + n^2 z &= f_z \end{aligned} \tag{3}$$

A force-free solution to Hill's equations is

$$\begin{aligned} x(t) &= \frac{\dot{x}_0}{n}\sin nt - \left(\frac{2\dot{y}_0}{n} + 3x_0\right)\cos nt + \left(\frac{2\dot{y}_0}{n} + 4x_0\right) \\ y(t) &= \frac{2\dot{x}_0}{n}\cos nt + \left(\frac{4\dot{y}_0}{n} + 6x_0\right)\sin nt + \left(y_0 - \frac{2\dot{x}_0}{n}\right) - (3\dot{y}_0 + 6nx_0)t \\ z(t) &= z_0\cos nt + \frac{\dot{z}_0}{n}\sin nt \end{aligned} \tag{4}$$

In terms of relative radial position and in-track velocity in Hill's reference frame, x and $\dot{y}$, the difference in semimajor axes (the ij subscript is subsequently omitted) is approximately given by

$$\Delta a \approx 2\left(2x + \frac{\dot{y}}{n}\right) = -(6nx + 3\dot{y})\left(\frac{-2}{3n}\right) \tag{5}$$

The differential semimajor axis is directly related to the secular drift term in the solution to Hill's equations, $-(6nx + 3\dot{y})t$, by a factor of $-2/(3n)$. If the difference in semimajor axes is zero, there will be no secular

drift between the spacecraft. The standard deviation of the differential semimajor axis estimate, $\sigma_{\Delta a}$, follows directly[4]

$$\sigma_{\Delta a} = 2\sqrt{4\sigma_x^2 + \frac{4}{n}\rho_{x\dot{y}}\sigma_x\sigma_{\dot{y}} + \frac{1}{n^2}\sigma_{\dot{y}}^2} \tag{6}$$

The parameters σ_x, $\sigma_{\dot{y}}$, and $\rho_{x\dot{y}}$ are derived from the error covariance matrix for the relative LVLH state estimate, $\hat{\mathbf{x}} = [\ x \quad y \quad \dot{x} \quad \dot{y}\ ]^T$ with estimation error $\tilde{\mathbf{x}} = \hat{\mathbf{x}} - \mathbf{x}$, which is assumed to be unbiased, $E[\tilde{\mathbf{x}}] = \mathbf{0}$, and have a covariance

$$E[\tilde{\mathbf{x}}\tilde{\mathbf{x}}^T] = \begin{bmatrix} \sigma_x^2 & \rho_{xy}\sigma_x\sigma_y & \rho_{x\dot{x}}\sigma_x\sigma_{\dot{x}} & \rho_{x\dot{y}}\sigma_x\sigma_{\dot{y}} \\ \rho_{yx}\sigma_y\sigma_x & \sigma_y^2 & \rho_{y\dot{x}}\sigma_y\sigma_{\dot{x}} & \rho_{y\dot{y}}\sigma_y\sigma_{\dot{y}} \\ \rho_{\dot{x}x}\sigma_{\dot{x}}\sigma_x & \rho_{\dot{x}y}\sigma_{\dot{x}}\sigma_y & \sigma_{\dot{x}}^2 & \rho_{\dot{x}\dot{y}}\sigma_{\dot{x}}\sigma_{\dot{y}} \\ \rho_{\dot{y}x}\sigma_{\dot{y}}\sigma_x & \rho_{\dot{y}y}\sigma_{\dot{y}}\sigma_y & \rho_{\dot{y}\dot{x}}\sigma_{\dot{y}}\sigma_{\dot{x}} & \sigma_{\dot{y}}^2 \end{bmatrix} \tag{7}$$

Note that if the radial position and in-track velocity are linearly correlated ($\rho_{x\dot{y}} = -1$), the expression for semimajor axis variance, from Eq. 6, reduces to

$$\sigma_{\Delta a} = 2\sqrt{4\sigma_x^2 - \frac{4}{n}\sigma_x\sigma_{\dot{y}} + \frac{1}{n^2}\sigma_{\dot{y}}^2} = 2\sqrt{\left(2\sigma_x^2 - \frac{1}{n}\sigma_{\dot{y}}\right)^2} \tag{8}$$

If the position and velocity error are linearly correlated and satisfy

$$\sigma_{\dot{y}} = 2n\sigma_x \tag{9}$$

then the position and velocity errors cancel and there is **no** error in the semimajor axis estimate. In other words, the two requirements for zero semimajor axis variance are:

$$\rho_{x\dot{y}} = -1 \quad \text{and} \quad \sigma_{\dot{y}} = 2n\sigma_x$$

which will subsequently be referred to as the correlation and balance requirements. In the examples, the balance is quantified with the *balance index*,

$$\texttt{bal} = \left|1 - \frac{2n\sigma_x}{\sigma_{\dot{y}}}\right| \tag{10}$$

which should be zero when the balance requirement is met. Note that if, instead, we have $\rho_{x\dot{y}} = 0$, then the expression for semimajor axis error reduces to

$$\sigma_{\Delta a} = 2\sqrt{4\sigma_x^2 + \frac{1}{n^2}\sigma_{\dot{y}}^2} \tag{11}$$

and in this case, $\sigma_{\Delta a}$ will not be zero unless both σ_x and $\sigma_{\dot{y}}$ are zero, which is not achievable.

The relationship between σ_x, $\sigma_{\dot{y}}$, $\rho_{x\dot{y}}$, and $\sigma_{\Delta a}$ is illustrated in Fig. 1.[4] The x and y axes of the plot are the standard deviations of the position and velocity estimation errors. Contours of constant semimajor axis standard deviation are shown on the figure. Each contour is associated with a value of $\rho_{x\dot{y}}$ in addition to a level of $\sigma_{\Delta a}$; several values of $\rho_{x\dot{y}}$ are shown for each level of $\sigma_{\Delta a}$. The diagonal of peaks indicates where $\sigma_{\dot{y}} = 2n\sigma_x$. Along the diagonal of peaks, the lines of constant semimajor axis experience a "bump" that increases in size as the correlation tends towards -1. This bump corresponds to increasing cancelation between the error in x and $\dot{y}$ that results from increasing correlation in these errors. Essentially, if the errors have high correlation and the proper balance, the higher error levels can be tolerated with the same resulting semimajor axis error. Each point on the graph corresponds to a unique set of σ_x and

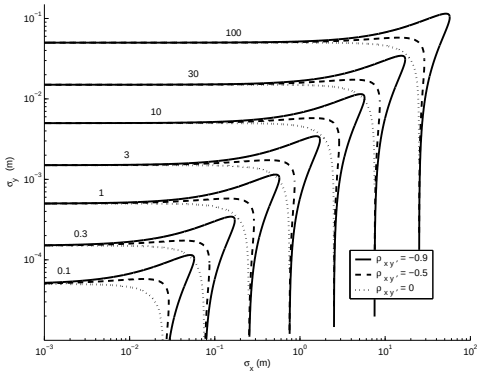

Fig. 1: Contours of constant semimajor axis vs. position and velocity accuracy. Contours given for 3 levels of correlation.

$\sigma_{\dot{y}}$. However, many points on the graph are intersected by more than one contour of constant semimajor axis. It is the correlation that determines the specific contour on which the system lies.

The analysis presented above was considered when exploring strategies to improve our CDGPS filter. Any navigation system that is not on the "bump" and does not have high correlation is not taking full advantage of the boost in semimajor axis knowledge that might otherwise be observed. Thus, making changes to meet the balance and correlation requirements should result in improvements to semimajor axis error. Unfortunately, the Kalman filter does not allow independent control over σ_x, $\sigma_{\dot{y}}$, and $\rho_{x\dot{y}}$. Further discussion of the relationship between typical values of σ_x and $\sigma_{\dot{y}}$ associated with Kalman filter output and corresponding $\rho_{x\dot{y}}$ and $\sigma_{\Delta a}$ is provided in the following section.

III. Semimajor Axis Accuracy from a Cartesian Filter Output

Theoretically, meeting the correlation and balance requirements described in Section II will result in perfect semimajor axis knowledge, so a design goal for a navigation system might be to achieve these requirements. In fact, Ref. 4 categorizes filters that meet the correlation requirement as "good." However, practical experience has shown that output from CDGPS filters typically does not meet these requirements, raising the questions of why the two requirements are not met and whether meeting these requirements should be a design goal.

In Ref. 11, Busse presents a Kalman filter using CDGPS measurements that achieves very good accuracies of ~ 1 cm position and ~ 0.5 mm/sec velocity. These results meet neither the balance nor the correlation requirements, with $\sigma_{\dot{y}}$ approximately twenty times larger than prescribed by the balance requirement, and the correlation coefficient is roughly -0.1. This suggests a discrepancy between the goal of having high correlation and the Kalman filter output reported in Ref. 11, which, under certain conditions is optimal. Note that extensive tuning of Q and R was done by Busse and in initial stages of this current work to produce the best possible estimate.

First, it must be determined whether a Kalman filter, by definition giving the best estimates of relative position and velocity,[8] produces the best estimate of semimajor axis difference. The relative semimajor axis is a linear combination of radial position and in-track velocity, as shown in Eq. 6. The nominal state vector, $\mathbf{x}_n$, can be transformed into a state, $\mathbf{x}_t$, that explicitly includes the semimajor axis,

$$\mathbf{x}_t = \begin{bmatrix} \Delta a \\ y \\ \dot{x} \\ \dot{y} \end{bmatrix} = \begin{bmatrix} 4 & 0 & 0 & 2/n \\ 0 & 1 & 0 & 0 \\ 0 & 0 & 1 & 0 \\ 0 & 0 & 0 & 1 \end{bmatrix} \begin{bmatrix} x \\ y \\ \dot{x} \\ \dot{y} \end{bmatrix} \equiv T\mathbf{x}_n \tag{12}$$

where T is the transformation matrix between the nominal state and the transformed state. Because T is full rank, its inverse exists. The state estimation error is defined as $\tilde{\mathbf{x}} = \hat{\mathbf{x}} - \mathbf{x}$, where $\hat{\mathbf{x}}$ is the state estimate. The estimation objective is related to the magnitude of the estimation error, which can be transformed as follows

$$\tilde{\mathbf{x}}_t^T \tilde{\mathbf{x}}_t = (\hat{\mathbf{x}}_t - \mathbf{x}_t)^T (\hat{\mathbf{x}}_t - \mathbf{x}_t) = (\hat{\mathbf{x}}_n - \mathbf{x}_n)^T T^T T (\hat{\mathbf{x}}_n - \mathbf{x}_n) = \tilde{\mathbf{x}}_n^T S \tilde{\mathbf{x}}_n \tag{13}$$

where $S = T^T T \geq 0$. From Ref. 8, the optimal estimate for the state $\mathbf{x}$ is found by minimizing the cost function $J = \mathtt{E}\left[\tilde{\mathbf{x}}^T M\ \tilde{\mathbf{x}}\right]$ where M is any positive semi-definite matrix. The key point is that the optimal estimate is *independent* of the choice of $M \geq 0$.[8] Since we can choose $M = I$, or $M = S$, as in Eq. 13, then the optimal estimate for $\mathbf{x}_t$ will be related to the optimal estimate for $\mathbf{x}_n$ by the linear transformation T. Thus, a Kalman filter estimating relative position and velocity *necessarily* will also yield the best possible estimate of the semimajor axis, to within the error associated with the linearization.

With this insight into the Kalman filter performance, the issue remaining is that the output does not fulfill the balance and correlation requirements. Note that if σ_x, $\sigma_{\dot{y}}$ and $\rho_{x\dot{y}}$ could be adjusted independently, the conditions for perfect semimajor axis knowledge could be met. However, there is no mechanism in the Kalman filter for adjusting these elements of the covariance matrix independently. Therefore, it is questionable whether the best strategy for achieving the lowest semimajor axis error is to require high correlation and good balance. In fact, the examples presented in the following sections, as well as experience with the CDGPS filter, suggest otherwise.

Table 1: Kalman Filter Elements for LPM Simulations

Description	**Notation**	**Simulation**
Dynamics Model	A	Planar Hill's Equations, constant in simulations
Measurements Model	H	Direct measures of position; GDOP varied by changing number and direction of measurements
Discrete Time Step	Δt	Varied
Process Noise	Q	Varied, to highlight effects of mis-modeled dynamics
Measurement Noise	R	Varied, to change quality of measurements

IV. A Linear Planar Model

If a Kalman filter produces the best estimate of the semimajor axis, but does not meet the balance and correlation requirements, this raises the questions of whether the filter can be forced to meet the requirements by adjusting the input parameters and whether this will improve semimajor axis knowledge. This investigation into the relationship between design parameters and navigation accuracy should also lead to a better understanding of what changes might be required to improve navigation. There are many parameters that must be specified for a Kalman filter, and all of these affect the accuracy of the estimates. Forces not captured in the dynamics model appear as process noise, and errors/nonlinearities in the sensors will affect the measurement noise. The dynamics and measurement models, the operating environment, and the extent to which nonlinearities are accentuated may all affect the process (Q) and sensor (R) noise intensities. The set of sensor data made available to the filter will determine the measurement matrix, H. Also, the time step can affect the performance of the discrete filter.

A CDGPS navigation filter has nonlinearities in both the system dynamics and the measurement equations, and because the set of visible GPS satellites changes, the measurement matrix H will change, and the state vector length will grow or shrink as the set of estimated carrier biases changes.[11] These factors make it difficult to understand direct relationships between the filter parameters and the navigational accuracies. Thus, we started with a simplified Linear Planar Model (LPM) to develop insights into the behavior of a relative navigation filter using CDGPS. Table 1 summarizes the Kalman filter parameters considered in the LPM simulations.

The system dynamics in this example were taken from the solutions of Hill's equations for radial and in-track position and velocity. Out-of-plane motion was ignored because it does not affect semimajor axis error. The dynamics model was not varied in the simulations, but its effective accuracy was modified by evaluating filter performance with different values of Q. Most GPS receivers can provide as many as twelve position-related range measurements. Similarly, the LPM includes two or more direct measures of position that span the orbital plane. Variations of the measurement model included changing the angle between the two position measurements and increasing the number of measurements included. Also the level of noise associated with one of the two measurements was changed. Different discrete time steps, Δt, were considered in these investigations. Note that as the time step changes, the relative importance of the dynamics model and the measurements will change. For example, if highly accurate measurements were provided at a very fast rate, the dynamics model might be of little importance. Conversely, once the estimate has converged, a perfect propagator might not need any future measurements. Changing the time step should illuminate how the filter might be tilted towards one of these extremes. The effects of changing the time step become more pronounced as nonlinear elements are introduced.

The simplified LPM problem is intended to show how each parameter in the problem affects the radial position error and in-track velocity error, the correlation of the two, and ultimately, the semimajor axis error. For each design variation, the position and velocity variances are found by numerically solving a discrete algebraic Riccati equation. The position and velocity error variances from the discrete Riccati equation (see Eq. 16) are used in Eq. 6 to compute the corresponding semimajor axis error.

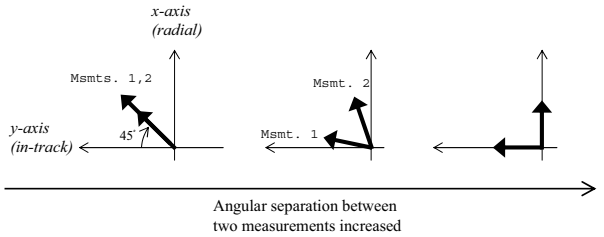

Fig. 2: LPM Example #1 – Filter performance as two measurements are brought into alignment.

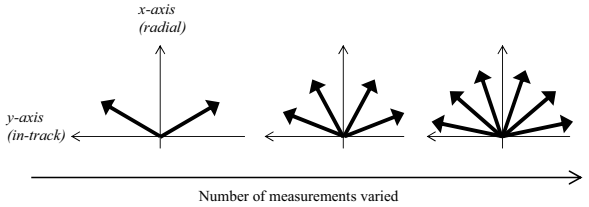

Fig. 3: LPM Example #2 – Filter performance as the number of measurements is varied.

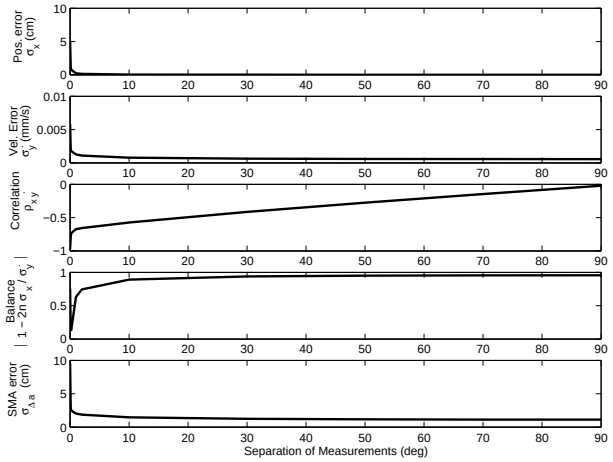

Fig. 4: LPM Example #1 – Filter performance versus angular separation

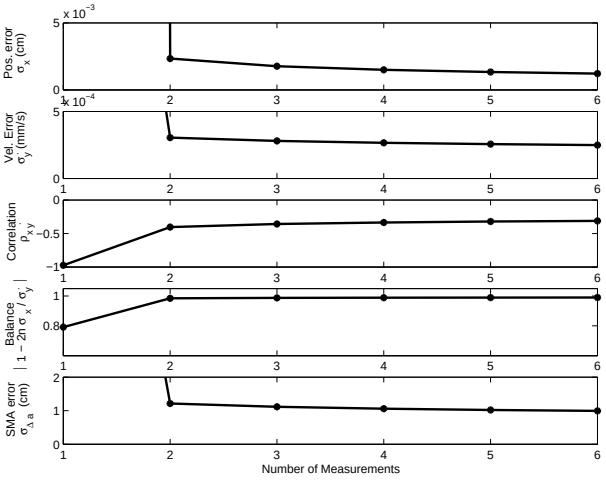

Fig. 5: LPM Example #2 – Filter performance versus number measurement

A. Two LPM Examples for Correlation Demonstrations

It is reasonable to expect the correlation between radial position and in-track velocity will increase only when the estimate depends more on the dynamics model embedded in the filter. This behavior is induced in examples that:

1. **Bring two measurements into alignment:** the angle between the two measurements is increased from 0° to 90°, as in Fig. 2. The direct observability of the orbital plane decreases as the two measurements become aligned, essentially causing the term $H^T R^{-1} H$ in the Kalman filter to drop rank. As a result the measurements will no longer span the full orbital plane, and the dynamics model must be employed to create the estimates of both states.

2. **Vary the number of measurements:** this example changes the direct observability by reducing the number of measurements from 1 to 6.

The results of examples one and two are discussed in the following.

Example #1: This example provides an excellent view of how the span of the measurement matrix affects the correlation and semimajor axis error. The two position measurements have equal accuracy and are initially aligned with the x and y axes. The angle between the two measurements is gradually decreased until the measurement directions are nearly collinear at a 45° angle in the $x - y$ plane. Fig. 4 shows that the correlation between the two remains low until the angular separation is less than ∼20°. When the angular separation becomes smaller than a degree, the correlation drops sharply from −0.7 towards −1. As the measurements approach alignment, the uniqueness of the information that each contributes decreases. The results show that the correlation rapidly approaches −1 as the dynamics become more important. However, when the measurements no longer span the orbital plane, the position and velocity errors increase dramatically. Since the balance requirement is not met exactly, the increased errors in position and velocity outweigh the advantage of the increased correlation, and the final semimajor axis error is large. In the

example shown, the two measurement directions converged on 45°, but similar results were seen for other terminal angles.

Example #2: This example looks at the effect of changing the number of measurements. They are equally spaced between 0° and 90° in the radial/in-track plane. The trends in this example, shown in Fig. 5, are consistent with the previous results. The values of σ_x and $\sigma_{\dot{y}}$ drop sharply, $\rho_{x\dot{y}}$ changes from close to -1 to around -0.5, and the balance index increases when the number of measurements is increased from 1 to 2. When the second measurement is added, the correlation and balance index are further from meeting requirements, but the semimajor axis knowledge improves. The results show that as additional measurements are added, the position and velocity errors continue to improve. Although the correlation decreases, the semimajor axis error improves when more information is used.

Discussion: In these examples, the filter can be made to rely on its dynamics model to extract good state information in the radial and in-track directions. This is accomplished by degrading the available sensing information. The increases in σ_x and $\sigma_{\dot{y}}$ that accompany the higher correlation consistently result in a larger semimajor axis error. This is a trait of a filter that is measurement dependent, not a symptom of a deficient one. When the correlation between radial position and in-track velocity is low, the best strategy for determining relative semimajor axis is to estimate both quantities with the highest possible accuracy and the Kalman filter does exactly that.

The behavior seen in both variations of this simplified example provide insight into the relative navigation system using CDGPS measurements. A GPS-based system will have many position related measurements available (around ten to twelve) that will be used by the filter. The GPS filter can also be forced to have better correlations by degrading the measurements and boosting the importance of the dynamics model. However, this results in increased semimajor axis error and is a sub-optimal strategy. Now that the LPM examples have shown that efforts to improve the navigation filter should not focus on $\rho_{x\dot{y}}$, the next section will transition to a full Nonlinear GPS Model (NGM) to explore what aspects of the filter contribute to the navigation accuracy.

B. LPM Simulations with Q and R

This section addresses the relationship between the Kalman filter parameters and the resulting estimate accuracy. These results are based on the premise that the Kalman filter produces the best answer from the given the models and measurements, and that the balance or correlation between elements of the state vector estimate are not important. Initial investigations showed that, predictably, the levels of measurement and process noise have the most influence of the estimate accuracy. These levels are indicators of how well the sensors and the dynamics are modeled. The relative levels of these noises determines how the filter will weigh new measurement information against the current state estimate propagated from the dynamics information.

Meeting the balance and correlation requirements discussed in Section III corresponds to being on the "bump" in Fig. 1, but the baseline results of the LMP simulation were above this region. This leads to the question of how changing filter inputs will move the output closer to or further from the bump. To answer this question, the LPM simulation was run for a range of measurement and process noise levels.

For each unique assignment of Q and R, the resulting error variances for radial position and in-track velocity, σ_x and $\sigma_{\dot{y}}$, were recorded. The corresponding semimajor axis error, $\sigma_{\Delta a}$, was calculated using Eq. 6. Fig. 6 shows lines of constant Q and R on axes of σ_x and $\sigma_{\dot{y}}$. The diagonal of peaks on this graph indicates the location of the "bump", where the balance and correlation requirements are met (which means $\sigma_{\dot{y}} = 2n\sigma_x$). By moving from one line of constant Q or R to another, one can see how decreasing the process or measurement noise would change the resulting position and velocity error. However, it is semimajor axis knowledge, not just position and velocity knowledge, that is important for control performance.

Several graphs demonstrate the relationship between Q, R and $\sigma_{\Delta a}$. First, Fig. 7 is reproduced and lines of constant semimajor axis error added. The lines for constant Q and R are dimmed for clarity. Note the lines of constant semimajor axis are horizontal, which corresponds with the horizontal sections of the semimajor axis contours on Fig. 1. The effect of changes in Q and R on $\sigma_{\Delta a}$ can be assessed by looking at the constant lines for all three values. Because the lines of constant semimajor axis are horizontal, improvement in $\sigma_{\Delta a}$ can only be accomplished by moving in the vertical direction on the graph, which is equivalent to decreasing $\sigma_{\dot{y}}$. Whether this requires decreasing Q or R depends on the angles between the horizontal lines of constant $\sigma_{\Delta a}$ and the contours of constant Q and R.

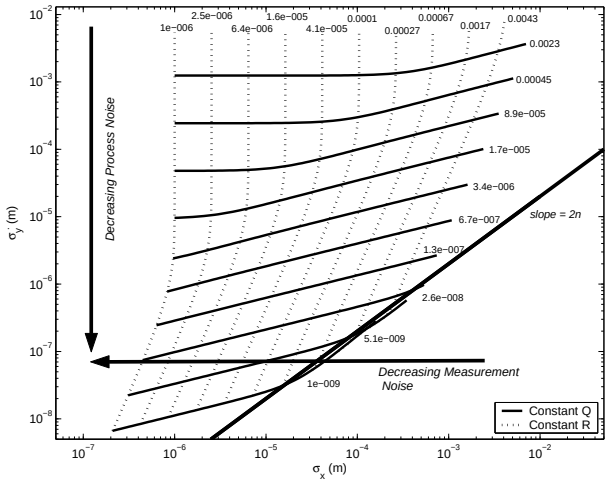

Fig. 6: Contours of constant Q and R are shown on axes of position and velocity accuracy.

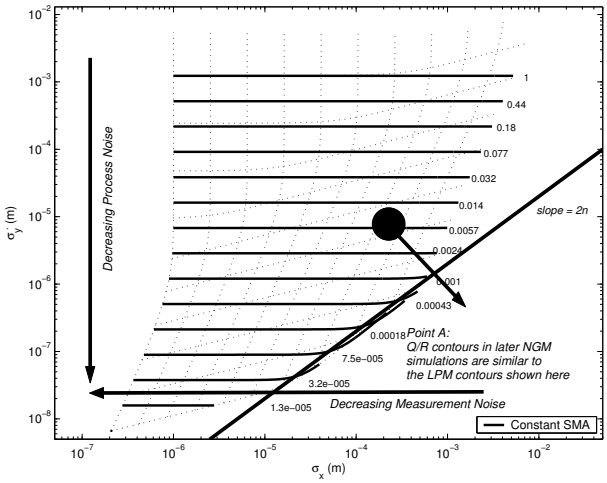

Fig. 7: Contours of constant semimajor axis shown vs position/velocity accuracy. Contours of constant Q and R are dotted lines in background.

Two regions are also indicated in Fig. 8. **Region 1** (upper left hand portion of the graph) contains lines of constant Q and R that are essentially horizontal and vertical, respectively. Improving the measurement noise in this region, or essentially moving horizontally in the graph, would have no effect on semimajor axis knowledge. Decreasing $\sigma_{\Delta a}$ would require improving the process noise to enable vertical movement on the graph. **Region 2** is closer to the line of $\sigma_{\dot{y}} = 2n\sigma_x$. Here, the lines of constant Q and R are no longer parallel and perpendicular to the horizontal lines of constant semimajor axis. This means that reducing either Q or R could improve $\sigma_{\Delta a}$. This shift from Region 1, where sensing improvement has no effect on $\sigma_{\Delta a}$, to Region 2, where it does, is also shown in Fig. 9 by plotting contours of constant semimajor axis on axes of Q and R. As expected, Region 1 has horizontal lines of constant $\sigma_{\Delta a}$, which directly shows that decreasing the measurement noise has little effect on semimajor axis knowledge. The portion of the graph where the contours of constant $\sigma_{\Delta a}$ are at an angle corresponds to Region 2. In this region, improvements in the measurements or the dynamics models (*i.e.* reduced process noise) would contribute to improved semimajor axis knowledge.

The LPM results shown thus far occupy the region above the $\sigma_{\dot{y}} = 2n\sigma_x$ line. Three questions arise: (i) What features of the system cause this behavior? (ii) Does this agree with expected behavior? (iii) What is required to cause the LPM results to move closer to this line, and below the line? In Region 1, $\sigma_{\Delta a}$ improvement requires decreasing $\sigma_{\dot{y}}$. This means that improvements in σ_x in this region have no effect on semimajor axis knowledge. In Region 1, the position error is smaller than the balance requirement dictates. This might be viewed as "excess" position accuracy with respect to determining semimajor axis. It is useful to consider what is driving the position and velocity accuracy in the GPS problem, and the representative LPM problem. Both models proposed a navigation system based on position measurements. In the LPM, the accuracy of the position estimate is then driven by the measurement noise. With no velocity measurement, the filter must obtain a velocity estimate from the derivative of the position estimate. Since this is tied to the dynamics model, it is reasonable to see velocity accuracy more closely associated with the process noise.

V. Agreement with Analytical Work

The LPM trends developed in Section B are now investigated analytically. The analysis, summarized below, develops analytical relationships between the process and measurement noise levels and the errors and correlations. The link between the two is established through the algebraic Riccati equation. The matrix Riccati equation has no known analytic solution for system more complicated than a double integrator. However, for a Kalman filter with a time step $\Delta t \approx 1$ second for a 90 minute orbit, the coupling between motion in the x and y directions is very weak and the dynamics can be well approximated as two weakly coupled double integrators. More formally, by defining $\epsilon = n\Delta t$, Hill's equations of motion can be rewritten

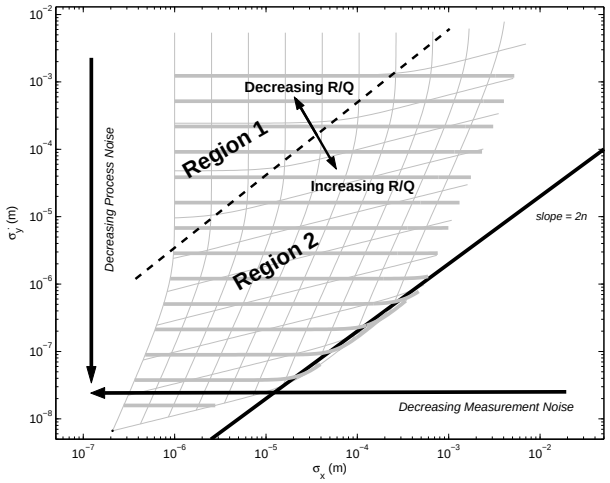

Fig. 8: In Region 1, decreasing the semimajor axis error requires decreasing the process noise level. In Region 2, decreasing either process or measurement noise can reduce semimajor axis error.

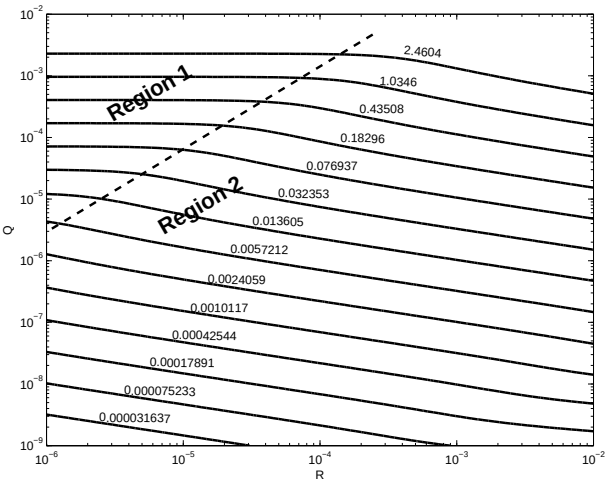

Fig. 9: Contours of constant semimajor axis shown against Q and R. In Region 1, process noise alone impacts the semimajor axis error, but in Region 2, both noise levels impact this error.

as

$$x'' = 2\epsilon y' + 3\epsilon^2 x + (\Delta t)^2 f_x \tag{14}$$
$$y'' = -2\epsilon x' + (\Delta t)^2 f_y \tag{15}$$

where $(*)' = (\dot{*})\Delta t$. When $\epsilon \ll 1$, which is true for this application, the x and y dynamics can be written as double integrators for which the solution of the Riccati equation is easily found. The combined dynamics then consist of two double integrators with coupling terms of order ϵ and ϵ^2. The measurements are of x and y. The variances σ_Q and σ_R refer to the standard deviation of the process and measurement noises. The process noise is assumed to be the same for all states and the measurement noise is assumed to be the same for all measurements.

The covariance for the full state is represented as Taylor expansion in ϵ. Substituting the expressions for $P = P_0 + \epsilon P_1 + \epsilon^2 P_2$ and $A = A_0 + \epsilon A_1 + \epsilon^2 A_2$ in the Riccati equation

$$\mathbf{0} = AP + PA^T + Q - PH^T R^{-1} HP \tag{16}$$

and grouping terms in the same power of ϵ, it is possible to solve for the expansion for the covariance matrix (P_{nxx}, $P_{n\dot{y}\dot{y}}$, and $P_{nx\dot{y}}$). To start, define $\mathbf{x} = [\ x \quad x'\ ]^T$ and $\mathbf{y} = [\ y \quad y'\ ]^T$. Then $P_{0\mathbf{xy}} = \mathbf{0}$ and

$$P_{0\mathbf{xx}} = P_{0\mathbf{yy}} = \begin{bmatrix} \sqrt{2}\sigma_Q^{\frac{1}{2}}\sigma_R^{\frac{3}{2}}\Delta t & \sigma_Q\sigma_R\Delta t^2 \\ \sigma_Q\sigma_R\Delta t^2 & \sqrt{2}\sigma_Q^{\frac{3}{2}}\sigma_R^{\frac{1}{2}}\Delta t^3 \end{bmatrix} \tag{17}$$

Substitution then gives that $P_{1\mathbf{xx}} = P_{1\mathbf{yy}}$=0 and

$$P_{1xy'} = -\frac{2\sigma_R^2 P_{0xx'}}{P_{0xx}} \quad P_{1x'y} = -P_{1xy'} \quad P_{1x'y'} = P_{1xy} = 0 \tag{18}$$

Then the correlation coefficient can be found from

$$\rho_{x\dot{y}} = \frac{P_{x\dot{y}}}{\sqrt{P_{xx}P_{\dot{y}\dot{y}}}} \approx \frac{\epsilon P_{1xy'}}{\sqrt{P_{0xx}P_{0y'y'}}} \tag{19}$$

Using the expressions given above, it follows that

$$\rho_{x\dot{y}} \approx -\frac{2(n\Delta t)\sigma_R^2(\sigma_Q\sigma_R\Delta t^2)}{\sqrt{2}\sigma_Q^{\frac{1}{2}}\sigma_R^{\frac{3}{2}}\Delta t}\left(\sqrt{2}\sigma_Q^{\frac{1}{2}}\sigma_R^{\frac{3}{2}}\Delta t\sqrt{2}\sigma_Q^{\frac{3}{2}}\sigma_R^{\frac{1}{2}}\Delta t^3\right)^{-1/2} = -\frac{\sqrt{2}\sigma_R^{3-\frac{3}{2}}\sigma_Q^{1-\frac{1}{2}}\Delta t^2}{\sqrt{2\sigma_Q^2\sigma_R^2\Delta t^4}} \tag{20}$$

$$\approx -n\sqrt{\frac{\sigma_R}{\sigma_Q}} \tag{21}$$

which, upon substitution in Eq. 6, gives a semimajor axis error of

$$\sigma_{\Delta a} = \frac{2}{n}\,\sigma_{\dot{y}} = \frac{2^{\frac{5}{4}}}{n}\,\sigma_Q^{\frac{3}{4}}\sigma_R^{\frac{1}{4}} \tag{22}$$

Eqs. 21 – 22 predict the correlation and semimajor axis error variance that can be expected from a Kalman filter. Since these predictions were developed from a model based on two double integrators, the results may not immediately map to the full CDGPS problem. However, these equations agree with LPM simulations.

To verify the ranges of σ_Q and σ_R for which the equation is valid. The correlation coefficient, $\rho_{x\dot{y}}$, has a limit of -1, so

$$-n\sqrt{\frac{\sigma_R}{\sigma_Q}} \geq -1 \quad \Rightarrow \quad \frac{\sigma_Q}{\sigma_R} \geq n^2 \tag{23}$$

In a low Earth orbit ($n \approx 0.001$), Eq. 23 implies that σ_R must be no more than six orders of magnitude larger than σ_Q. With this insight, the LPM model was evaluated for a wide range of σ_Q and σ_R, and the "true" semimajor axis variance was calculated using Eq. 6. This true value was compared to both forms of the prediction error given in Eq. 22. The true correlation was calculated using the covariance matrix from the Riccati solver, as defined in Eq. 7. The percentage errors for all three comparisons were found to be very small, indicating very good agreement between the prediction equations and LPM simulation results.

Note that Eq. 21 requires that the process noise be a million times smaller than the sensor noise. Many space-rated GPS receivers produce differential carrier phases measurements with millimeters of error. To achieve $\rho_{x\dot{y}} = -1$, the dynamics environment of the vehicle would have to be modeled to nanometer-level accuracy, which is not currently possible. This interpretation of the relationship between correlation and process and measurement noises concurs with conclusions drawn from the LPM examples.

VI. A Nonlinear GPS Model

The LPM simulations provided a baseline of the expected behaviors from the Nonlinear GPS Model simulations and an indication of what parameters to vary. As in the LPM experiments, the NGM was simulated for an array of values of Q and R. For each set of Q and R, the full GPS simulation was run for 3000 seconds, to allow sufficient time for the filter to converge to steady state. The absolute truth states for the vehicles were propagated to create the simulated GPS measurements and differenced to create the relative state truth. The position and velocity errors were determined from the standard deviation of the estimation error, not from a Riccati equation as in the LPM cases. Note that in the nonlinear case, Eq. 6 was found to give inaccurate estimates of the semimajor axis error, so the orbital elements for the two vehicles were calculated. The absolute semimajor axes were differenced at each time step and the differential semimajor axis errors were stored. The square root of the variance of these estimation errors (after the filter had converged) was recorded.

The simulation software for the NGM model propagates the orbit and provides simulated measurements to the estimator. Because a large number of simulations was required to observe relationships between filter parameters and the navigation accuracy, it was not practical, or perhaps even possible, to employ hardware-in-the-loop simulations. Generally, the software simulations produce results that are more accurate than the hardware simulations. However, previous and current work has observed that trends seen in the software simulations are also seen in the hardware simulations.

The NGM simulation tools were originally developed by Busse,[10] and were modified as needed for this work. The user has a great deal of control over how nonlinear effects and perturbations are modeled in the truth propagator and are accounted for in the filter. This is very useful in trying to relate the NGM to the LPM, because the NGM with no nonlinearities or perturbations should approach the LPM. The initial nonlinear effects are reduced by placing the vehicles 1 meter apart. This minimizes truncation error in the relative orbital dynamics equations. It also causes the line-of-sight vectors to the GPS satellites for the two vehicles to be nearly identical, which is another assumption made by the filter.

Three NGM simulations illustrate the relationship between noises and estimator performance. The goal of the first simulation is to create a model that has the full NGM state, with clock and carrier bias terms included, and that uses simulated GPS measurements, but that also looks as much like the LPM as possible. To accomplish this, many real-world effects that are usually included in software simulations, such as ephemeris error, clock error, communication outages, and measurement cycle slips, are not included. The first simulation is run at a 0.1 second time step. The second simulation, run at a 1 second time step, is

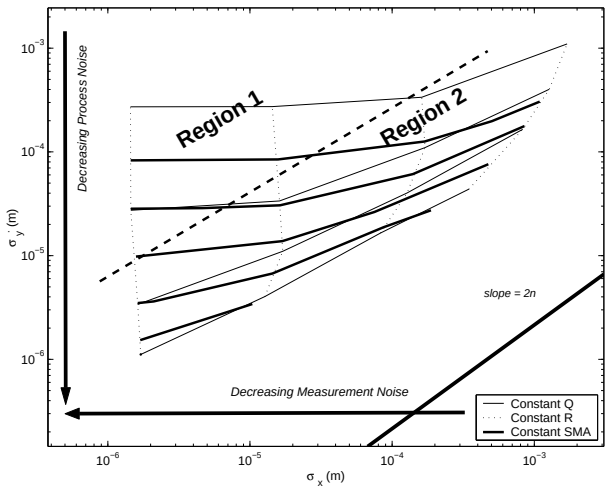

Fig. 10: Contours of constant Q, R and semimajor axis are shown for NPM results. Nonlinear effects were minimized for this simulation, which was run with a 0.1 second time step.

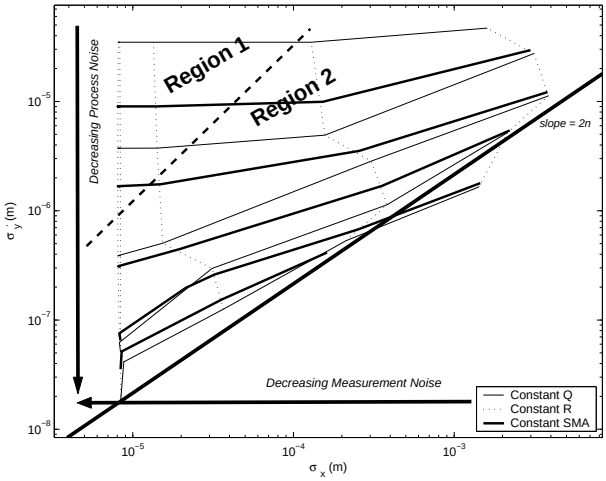

Fig. 11: Contours of constant Q, R and semimajor axis are shown for NPM results. Clock, ionospheric, and absolute state errors were removed in this simulation, which had a 1 second time step.

intended to be an intermediate step between an unrealistic, nearly linear simulation, and the fully nonlinear simulation that models real world error sources. It also introduced very low levels ephemeris errors and clock errors. The third NGM simulation, also at a 1 second time step, included all available error sources in the models for the environment and sensors.

A. NGM Simulations with Q and R

The NGM analysis begins with a very simple model that focuses on the relative orbital dynamics and GPS measurements, and takes steps to reduce nonlinearities associated with their equations. Starting with such a simple model has two main advantages. First, the simple NGM model, like the LPM, uncovers the basic relationships between process and measurement noises and semimajor axis error. Second, starting with the very simple model allows the trends caused by clock, ephemeris, and other extraneous errors to be identified.

The first NGM simulation removes most of the simulated errors to begin with a problem that is most like the LPM. To further reduce the importance of the nonlinearities that the NGM dynamics model introduces, the filter is run at a 0.1 second time step. Fig. 10 shows contours of constant Q, R and $\sigma_{\Delta a}$ that are very similar to the LPM. As in the LPM, Region 1 contains lines of constant Q and R that are essentially horizontal and vertical. Improving the measurement noise in this region would have no effect on semimajor axis knowledge. Reductions in process noise are required to reduce $\sigma_{\Delta a}$. In Region 2, improvements in the measurements or the dynamics models would contribute to improved semimajor axis knowledge.

An interesting change was observed in the second simulation, when the time between measurement updates was increased to 1 second. In the first NGM simulation and the LPM simulation, the lines of constant R bent to the left at the bottom. In the second NGM simulation, in Figure 11, the lines of constant R bend to the right before turning back left. This would mean that improving process noise and keeping the measurement noise constant results in improved velocity accuracy, but causes the position accuracy to actually degrade. This change reflects the increased effect of the dynamics nonlinearities.

However, the second simulation retains the major trends of the first NGM simulation and the LPM. In Region 1, constant measurement noise contours are vertical, and constant contours for process noise and semimajor axis are horizontal. This means that process noise reductions are required to improve semimajor axis knowledge, and measurement noise reductions have no impact. In Region 2, the lines of constant Q are similar to the LPM model, starting horizontal and sloping upwards slightly near the line of $\sigma_{\dot{y}} = 2n\sigma_x$. The tops of the contours of R share the vertical orientation seen in the LPM, though, as discussed above, nonlinear effects begin to reshape the bottom sections of the contours.

The final NGM simulation includes errors introduced by clock, ephemeris, and absolute state uncertainty, which were excluded from the first two simulations. Fig. 12 shows constant lines of Q, R and $\sigma_{\Delta a}$ on axis of σ_x and $\sigma_{\dot{y}}$. The line of $\sigma_{\dot{y}} = 2n\sigma_x$ is included as a reference, but will not necessarily represent the same transition point that it did in the LPM. The region that coincides with typical CDGPS accuracy is indicated on the plot.

Contours of constant process noise tend to the horizontal direction and contours of constant measurement noise tend towards vertical. The contours of constant semimajor axis have a mildly positive slope, but are still fairly similar to the contours seen on the LPM plots.

The trends for constant Q, R lines are in general agreement with the LPM plots, in the sense that both show upward titled parallelograms (see Point A in Figs. 7 and 12). In going from the LPM to the NGM, the horizontal lines of constant semimajor axis become slightly sloped. This indicates that position accuracy will have some effect on $\sigma_{\Delta a}$ in the NGM, where it had no effect in the LPM. The slope of the NGM contours is still small, which indicates the velocity error will still dominate semimajor axis knowledge.

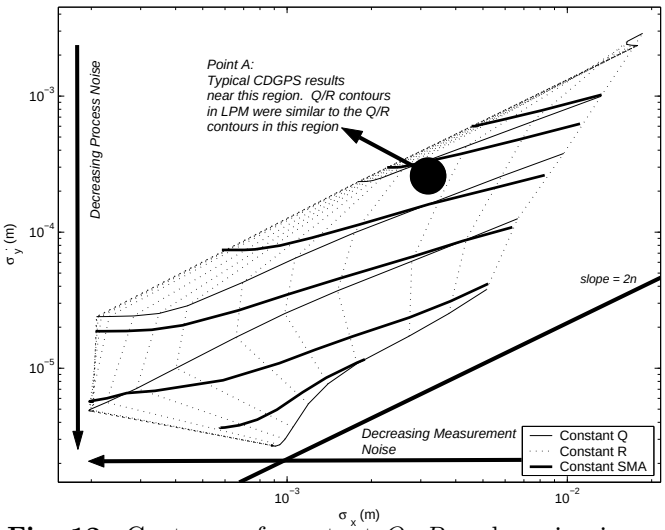

Fig. 12: Contours of constant Q, R and semimajor axis are shown for NPM results. This NPM included clock, ionospheric, and absolute state errors.

The major departure from LPM behavior is seen in the lines of constant measurement noise. In the LPM case, reducing measurement noise always resulted in reductions of σ_x. In Region 1 of the LPM, Fig. 8, the lines of constant R were vertical and orthogonal to the lines of constant semimajor axis. In this region, decreasing R would not improve $\sigma_{\Delta a}$, but, improvements to σ_x were always possible. In the NGM cases, the contours of constant R begin to bunch when they become very small. This implies that further reductions will impact neither $\sigma_{\Delta a}$ nor σ_x. The fact that σ_x does not continue to improve as the measurement noise is decreased suggests that some aspect of the NGM that models realistic phenomenon, such as clock error, is limiting the overall accuracy.

Fig. 12 suggests several things about the performance of our CDGPS-based relative navigation filter. Reducing either process or measurement noise can have a positive effect on semimajor axis. The stance taken in the development of prior work was that a coarse dynamics model is sufficient because measurement updates are performed very frequently.[10] To a large degree, that assumption was correct. The performance of that filter was very good and met the stated requirements. Still, this analysis suggests that future work to incorporate a higher fidelity dynamics model, thereby reducing the process noise, could improve the semimajor axis knowledge. Finally, this analysis shows that noise from sources besides the CDGPS measurements and the relative orbital dynamics model, such as from the clock and absolute state error, also impacts the performance. When these errors are introduced, there is a limit to how much the position, velocity, and semimajor axis performance can be improved. It is expected that there should be a limit to how much velocity and semimajor axis can be improved by increasing the sensor accuracy. However, in the LPM, sensor improvement always resulted in improved position accuracy, which is not true for the NGM.

The progression of the simulations describe above shows the Linear Planar Model, analyzed in the previous section, gradually being changed into a fully nonlinear example. Nonlinearities in measurement and dynamics, perturbations in the environment, and uncertainty introduced by an inaccurate vehicle clock bend the contours of constant Q and R to some degree. However, the general trends, especially in the area where typical CDGPS filters are found, are retained. The similarities between the linear and nonlinear results suggest that the insights gained from the LPM examples about the relationships between correlation and errors, and between process and measurement noises and errors are relevant to the more complex CDGPS filters.

VII. Conclusion

This paper was motivated by the desire to 1) determine what metrics should be used to characterize the filter performance as "good," and 2) explore what parameters in the Kalman filter have the most impact on the performance of the navigation system. Closed loop control performance, which the navigation system exists to support, is dependent on accurate knowledge of the semimajor axis. This paper showed that a Kalman filter estimating relative position and velocity will also produce the best estimate of the differential semimajor axis, because these quantities can be related by a linear transformation.

Previous research has suggested that if the position and velocity errors have high correlation and the proper balance, semimajor axis error can effectively be canceled out, but this idea did not concur with previous and current experience with CDGPS-based navigation systems. Two examples based on a linear planar model were presented to show that the standard GPS problem could be modified to yield highly correlated estimates, but this was always accompanied by an increase in the semimajor axis error. This is because the Kalman filter does not allow independent control over σ_x, $\sigma_{\dot{y}}$, and $\rho_{x\dot{y}}$, which is required to meet both the correlation and balance requirements.

The simple linear model was then used to explore how the filter design parameters affect the navigation accuracy, and the results showed the relationship between the filter inputs, measurement and process noise, and the filter output (navigation errors and their correlation). The simulation results were shown to match a recently derived analytic expression for the correlation coefficient. Similar tests were done using a full nonlinear GPS simulation. The general trends seen in the linear model were retained in the nonlinear results, suggesting that the insights gained from the linear examples are valuable in understanding complex CDGPS filters. The differences in the linear and nonlinear simulations were also investigated, and these highlighted the effects that realistic phenomenon, such as clock and ephemeris error, have on the performance of the filter.

Acknowledgments

This work was funded under Cooperative Agreement NCC5-729 through the NASA GSFC Formation Flying NASA Research Announcement. Any opinions, findings, and conclusions or recommendations expressed in this material are those of the authors and do not necessarily reflect the views of the National Aeronautics and Space Administration.

References

[1]J. Leitner, F. Bauer, D. Folta, M. Moreau, R. Carpenter, J. How, "Distributed Spacecraft Systems Develop New GPS Capabilities," in *GPS World: Formation Flight in Space* Feb. 2002.

[2]F. H. Bauer, J. O. Bristow, J. R. Carpenter, J. L. Garrison, K. Hartman, T. Lee, A. Long, D. Kelbel, V. Lu, J. P. How, F. Busse, P. Axelrad, and M. Moreau, "Enabling Spacecraft Formation Flying through Spaceborne GPS and Enhanced Autonomy Technologies," in *Space Technology*, Vol. 20, No. 4, p. 175–185, 2001.

[3]M. Tillerson, G. Inalhan, and J. How, "Coordination and Control of Distributed Spacecraft Systems Using Convex Optimization Techniques," *Int. Journal of Robust and Nonlinear Control*, vol 12, Issue 2-3, Feb.-Mar. 2002, p.207-242.

[4]J. R. Carpenter and K. T. Alfriend, "Navigation Accuracy Guidelines for Orbital Formation Flying," AIAA G*uidance, Navigation, and Control Confrence*, Austin, TX, Aug 11-4, 2003.

[5]J.R. Carpenter, E. Schiesser, "Semimajor Axis Knowledge and GPS Orbit Determination," in *Journal of the Institute of Navigation* Vol. 48, No. 1, Spring 2001.

[6]J. How and M. Tillerson, "Analysis of the Impact of Sensor Noise on Formation Flying Control," Proceedings of the *American Control Conference*, June 25-27, 2001, p. 3986-3991.

[7]M. Kaplan. *Modern Spacecraft Dynamics and Control*. Wiley, 1976.

[8]A. Gelb. *Applied Optimal Estimation*. MIT Press, 1974.

[9]M. Grewal, A. Andrews. *Kalman Filtering*. Wiley, 2001.

[10]F. Busse, "Precise Formation-State Estimation in Low Earth Orbit Using Carrier Differential GPS," Ph.D. Dissertation, Stanford University, Dept. Aeronautics and Astronautics, Feb. 2003.

[11]F. D. Busse, J. Simpson, and J. P. How, "Demonstration of Adaptive Extended Kalman Filtering for LEO Formation Estimation Using CDGPS," *Navigation* Journal of the Institute of Navigation, Vol. 50, No. 2, Summer 2003, pp. 79–94.